International Journal of Solids and Structures 81 (2016) 33–42

Contents lists available at ScienceDirect

International Journal of Solids and Structures

journal homepage: www.elsevier.com/locate/ijsolstr

On the conical indentation response of elastic auxetic materials: Effects of Poisson's ratio, contact friction and cone angle

D. Photiou, N. Prastiti, E. Sarris, G. Constantinides*

Research Unit for Nanostructured Materials Systems, Department of Mechanical Engineering and Materials Science and Engineering, Cyprus University of Technology, 3041 Lemesos, Cyprus

ARTICLE INFO

Article history:
Received 28 May 2015
Revised 25 September 2015
Available online 2 December 2015

Keywords:
Indentation
Auxetic materials
Contact mechanics

ABSTRACT

The linear elastic analytical solution of an axisymmetric probe indenting a semi-infinite half-space forms the backbone of most indentation data analysis protocols. It has been noted in the literature that the theoretical solution relies on a boundary condition that is ill-posed which leads to discrepancies from the actual response that depends, among other parameters, on the Poisson's ratio of the indented material. While correction factors have been proposed, prior studies have concentrated on the positive Poisson's ratio regime and have neglected an exciting and developing class of materials: the auxetic systems. The finite element method is used to simulate the conical indentation response of elastic materials with Poisson's ratios covering the whole thermodynamically possible range, $-1 \le \nu \le 0.5$. Consistent with theoretical predictions, the indentation resistance and hardness of auxetic materials is enhanced compared to their non-auxetic counterparts. The stress profiles and contact details are systematically analyzed and the increase in resistance is traced to the shear stiffening and the reduction of contact area compared to conventional materials. Furthermore, it is shown that the analytical linear elastic solution falls short in accurately describing the indentation response, especially for negative Poisson's ratio materials. In contrast to the theoretical prediction, the contact area reduces as the Poisson's ratio increases resulting in increased required force to penetrate the material and an enhanced pressure distribution beneath the indenter. The analytical solution is corrected for the whole ν range and best fit polynomials are proposed for ease-of-use. The effects of contact-friction and indenter cone-angle are also studied and quantified.

1. Introduction

Instrumented indentation has developed into a standardized tool for nano- and micro-mechanical characterization of materials (Bulychev et al., 1975; Doerner and Nix, 1986; Fischer-Cripps, 2002; Oliver and Pharr, 2011,1992). It was initially introduced for characterizing thin films and sub-micron material volumes but it has expanded its application range into studying virtually all classes of material systems: metals (Schuh, 2006; Tabor, 2000), ceramics (Cook and Pharr, 1990; Lawn, 1998; Wachtman et al., 2009), polymers (Tweedie et al., 2007; Vandamme et al., 2012; VanLandingham et al., 2001) and composites (Constantinides et al., 2009, 2006, 2003; Němeček et al., 2013).

The current state of hardware and electronics ensures that loads and displacements can be recorded with nN and angstrom scale resolutions, respectively, and force-displacement curves are nowadays routinely collected either in the nanometer or micrometer regime. An equally important step in the nanomechanical characterization of materials is the conversion of experimental data into meaningful material properties. There are several analytical approaches for completing this step most of which have focused on the indentation modulus ($E*$) and hardness (H) of the material:

$$E^* = \frac{\sqrt{\pi}}{2}\frac{S}{\sqrt{A_c}} \tag{1}$$

$$H = \frac{P_{\max}}{A_c} \tag{2}$$

where S is the unloading slope at maximum depth ($h_{\max}$), $S = dP/dh|_{h_{\max}}$, A_c is the area of contact at maximum load ($P_{\max}$). $E*$ and H, under certain circumstances, can be converted to the elastic modulus (Borodich and Keer, 2004a, 2004b; Pharr et al., 1992) and strength characteristics (Cariou et al., 2008; Ganneau et al., 2006; Tabor, 2000) of the indented system. In the case of a rigid indenter $E*$ relates to the plane stress modulus of the material, $E^* = \frac{E}{(1-\nu^2)}$

Directly or indirectly most analysis methods make use of the analytical solution of an axisymmetric indenter being pushed against a semi-infinite, linear elastic half-space. In fact Eq. (1) can be directly

* Corresponding author. Tel.: +357 25002626; fax: +357 25002666.
E-mail address: g.constantinides@cut.ac.cy (G. Constantinides).

http://dx.doi.org/10.1016/j.ijsolstr.2015.10.020
0020-7683/

derived from the linear elastic solution (Bulychev et al., 1975; Oliver and Pharr, 1992) and it has been proven that it holds true for any indenter that can be described as a solid of revolution (Pharr et al., 1992). Impressively enough, the equation is still valid even if the material exhibits elastic–plastic response with the only provision that the area of contact is properly accounted for in the analysis (Cheng and Cheng, 1997). In other words all plasticity phenomena are incorporated into the area of contact and provided that this is accurately captured, Eq. (1) continues to hold.

Several finite element studies (Bolshakov and Pharr, 1998; Cheng and Cheng, 1999, 1998; Dao et al., 2001; Troyon and Huang, 2011) have pointed out that computational results deliver consistently higher values of the modulus of elasticity when calculated through Eq. (1). A detailed analysis by Hay et al., (1999) in her, by now, classic paper of 1999 has deciphered the origins of this discrepancy which has its roots on an inaccurate boundary condition used in the formulation of the mathematical problem that has been analytically solved (see Section 2); the issue of tangential displacements has also been reported in several other studies (Argatov, 2004; Kindrachuk et al., 2009), see also discussion and references in Borodich (2014)). Through finite element modeling they have quantified this uncertainty and they have formulated analytical approximations for a correction factor γ for Eq. (1) based on simple modifications of Sneddon's solution, which proved to be a function of Poisson's ratio of the material (ν) and the cone semi apex angle (θ):

$$E^* = \frac{1}{\gamma}\frac{\sqrt{\pi}}{2}\frac{S}{\sqrt{A_c}} \tag{3}$$

$$\gamma = 1 + \frac{\beta}{4\tan\theta} \tag{4}$$

$$\gamma = \pi\frac{\frac{\pi}{4} + 0.15483073\cot\theta\frac{\beta}{4}}{\left(\frac{\pi}{2} - 0.83119312\cot\theta\frac{\beta}{4}\right)^2} \tag{5}$$

where $\beta = \frac{1-\nu}{1-2\nu}$. Eq. (4) is best suited for cube-corner indenters whereas Eq. (5) for Berkovich/Vicker-type geometries. While correction factors have already been proposed (Hay et al., 1999; Poon et al., 2008; Xu, 2008), the majority of studies (with a few recent analytical exceptions (Argatov and Sabina, 2014; Argatov et al., 2012) have concentrated in the positive Poisson's ratio regime and have neglected an exciting and developing class of materials: the auxetic systems. The thermodynamic constrains on the materials elastic properties allow for Poisson's ratio of the material to move into the negative domain, more specifically $-1 \le \nu \le 0.5$. This leads to the counter-intuitive behavior, in which materials tend to expand in the lateral dimension in response to stretching. This geometrically/kinematically-driven response to loading leads to an increase in volume and thus materials that fall into this category have been termed auxetic. Equivalently the same materials will tend to reduce their volume when compressed (thus miotic). Ever since the experimental reporting of such a response by re-entrant structures polyurethane in 1987 by Lakes (1987), many other systems have been found to exhibit similar deformation patterns. Most of these systems fall into man-made or naturally occurring microporous systems like polytetrafluoroethylene (Lakes, 1987), microporous ultra high molecular weight polyethylene and polypropylene (Alderson et al., 2000, 1994), various types of rocks and crystals (Zouboulis et al., 2014), a-cristobalite (Grima et al., 2005), zeolites (Gatt et al., 2008), various laminate composites (Milton, 1992), defected graphene (Grima et al., 2015), and many others. For a more detailed exposition of this particular material behavior the reader is referred to the reviews of Lakes (1993), Yang et al. (2004) and Greaves et al. (2011).

The finite element method is used in this paper to simulate the conical indentation response of elastic materials with Poisson's ratios covering the whole thermodynamically possible range, $-1 \le \nu \le 0.5$. The aim of this particular study is twofold: on one side we aim to quantify the increased indentation resistance reported in the literature when indenting auxetic materials and identify through computational simulations the mechanisms that lead to this particular response. On the other hand we aim to deal with the discrepancy caused by the existing analytical solution when indenting auxetic materials and extract correction factors that will eliminate any inaccuracies and will correct the analytical solution for the entire possible span of Poisson's ratios.

2. Theoretical background

The main focus of contact mechanics is the determination of size and exact shape of the contact area. Unlike classical mechanics problems, the contact zone is unknown so that areas where displacements (in the contact region), and those where forces (free surface) are prescribed are not known *a priori*. This renders the analysis intrinsically non-linear, since the surface boundary conditions have to be formulated under restrictions of a point z that is either situated in the contact zone or in the stress-free area. The contact problem between a rigid axisymmetric indenter and an infinite half-space is described by the following set of equations, written in polar coordinates (ρ, φ, z):

$$div\,\sigma = 0 \tag{6}$$

$$\sigma = F(\varepsilon) \tag{7}$$

$$\varepsilon = \frac{1}{2}\left(\nabla u + \nabla^t u\right) \tag{8}$$

$$P = -\int_{\rho=0}^{a}\int_{\theta=0}^{2\pi}\sigma_{zz}(\rho,\varphi,0)\rho d\rho d\varphi \tag{9}$$

$$u_z(\rho,\varphi,0) = -h + f(\rho);\ \rho < \alpha \tag{10}$$

$$\sigma_{\rho z}(\rho,\varphi,0) = 0;\ \rho > 0 \tag{11}$$

$$\sigma_{zz}(\rho,\varphi,0) = 0;\ \rho > a \tag{12}$$

where P is the applied load, in direction z, $f(\rho)$ defines the axisymmetric shape of the indenter, and a is the contact radius. Eq. (6) is the static equilibrium condition, Eq. (7) provides the stress–strain relation of the indented material (here linear isotropic elastic), Eq. (8) links strain to displacements and the remaining relations (Eqs. (9)–(12)) are the boundary conditions for the total load (Eq. (9)), the vertical displacement in the contact region (Eq. (10)), the zero shear stress on the surface (Eq. (11)) which includes the frictionless contact condition and the stress-free boundary condition outside the contact zone (Eq. (12)).

There are several ways of solving the above set of equations, the more traditional one being the method developed by Lee and Radok (1960), and further formalized by Sneddon (2010) and (1965) which consists in performing on all problem equations two dimensional Fourier transforms in the directions of the surface coordinates x and y. In the case of axi-symmetry, this integral transform is called a Hankel transform on the polar coordinates ρ and φ which are transformed into a variable φ of dimension L^{-1}. The area of contact is circular by symmetry and its projected radius a is kept as an unknown. It turns out that the equations written with a new set of non-physical coordinate can be solved analytically in the transformed space. Finally the integral transforms are performed backwards to return to the original problem. Following this procedure, the expressions for h and P for an isotropic half-space read:

$$h = \alpha\int_{\rho=0}^{\alpha}\frac{f'(\rho)d\rho}{\sqrt{a^2-\rho^2}} \tag{13}$$

$$P = 2\frac{E}{1-\nu^2}\int_{\rho=0}^{\alpha}\frac{\rho^2 f'(\rho)d\rho}{\sqrt{a^2-\rho^2}} \tag{14}$$

where f is any smooth convex function, and f' stands for its derivative with respect to ρ. The origin of Eqs. (13) and (14) can be traced back the work of Galin in 1946 (see references and discussion in Borodich(2014)). This result implicitly relies on an assumption about the contact area, through a. By inverting Eqs. (13) and (14), the contact radius α can be expressed as a function of the prescribed depth h or load P. The displacements in the half space are given by:

$$u_\rho(\rho,z)=\frac{1}{2(1-\nu)}\int_0^\infty(1-2\nu-\xi z)A(\xi)e^{-\xi z}J_1(\rho\xi)d\xi \tag{15}$$

$$u_z(\rho,z)=\frac{1}{2(1-\nu)}\int_0^\infty(2-2\nu+\xi z)A(\xi)e^{-\xi z}J_0(\rho\xi)d\xi \tag{16}$$

where $A(\xi)$ depends on the shape of the indenter and J_0, J_1 are Bessel functions of the first kind. We here present the solutions of Eqs. (13)–(16) for an axisymmetric indentation with a cone of semi-apex angle of θ for which

$$f(\rho)=\frac{\rho}{\tan\theta} \tag{17}$$

In this case,

$$A(\xi)=\frac{1}{\tan\theta}\frac{1-\cos\alpha\xi}{\xi^2} \tag{18}$$

and

$$u_\rho(\rho<a,0)=\frac{\beta}{4}\frac{\rho}{\tan\theta}\left[\ln\frac{\rho/\alpha}{1+\sqrt{1-\left(\frac{\rho}{\alpha}\right)^2}}-\frac{1-\sqrt{1-\left(\frac{\rho}{\alpha}\right)^2}}{\left(\frac{\rho}{\alpha}\right)^2}\right] \tag{19}$$

$$u_\rho(\rho>a,0)=\frac{1}{\tan\theta}\left[\alpha\sin^{-1}\frac{\alpha}{\rho}+\sqrt{\rho^2-\alpha^2}-\rho\right] \tag{20}$$

$$\sigma_{zz}(\rho<\alpha,0)=\frac{1}{2\tan\theta}\frac{E}{1-\nu^2}\cosh^{-1}\left(\frac{\alpha}{\rho}\right) \tag{21}$$

Eq. (21) shows a stress singularity for $\rho=0$ right below the tip of an infinitely sharp cone. This is not the case for smooth indenters, but it appears in the case of a flat punch for $\sigma_{\rho z}(\rho=a,0)$. Eqs. (20) and (21) provide explicit relations of depth and load as a function of the contact radius:

$$h=\frac{\pi}{2}\frac{\alpha}{\tan\theta} \tag{22}$$

$$P=\frac{\pi}{2}\frac{E}{1-\nu^2}\tan\theta h^2 \tag{23}$$

As expected from dimensional analysis, P is scaled with h^2, which provides an interesting insight into the nonlinear nature of the contact problem: for each increment of load, both the area of contact and the depth of indentation increase. Similarly, a and h are linearly related and can define the contact depth as the distance measured on the z-axis between the indenter tip and the contact edge. From Eq. (22) we obtain the following relation:

$$h_c=\frac{\alpha}{\tan\theta}=\frac{2}{\pi}h \tag{24}$$

Eq. (24) suggests that the elastic indentation always produces sink-in. In fact, provided that the material remains purely elastic the contact depth to indentation depth ratio will always be a constant at $h_c/h=2/\pi=0.64$. Furthermore, if one rewrites P and h in Eqs. (22) and (23) as a function of the projected area of contact $A_c=\pi a^2$, then one obtains:

$$h=\frac{\sqrt{\pi}}{2}\frac{\sqrt{A_c}}{\tan\theta} \tag{25}$$

$$P=\frac{1}{2}\frac{E}{1-\nu^2}\frac{A_c}{\tan\theta} \tag{26}$$

Eq. (26) suggests that the hardness of the material is constant and independent of the depth of penetration:

$$H=\frac{P}{A_c}=\frac{1}{2\tan\theta}\frac{E}{1-\nu^2} \tag{27}$$

We reiterate that the above solution relies on a linear elastic form of the constitutive relations, Eq. (7), and is therefore only valid for linear elastic solids. Furthermore, the solution presented above implicitly relies on the restriction posed on the vertical displacements at the contact interface described by Eq. (10). The radial movements of the indented surface have been neglected, leading to deformed geometries that essentially 'penetrate' the indenter during loading (Hay et al., 1999), resulting in inaccuracies on the predicted load and interfering with any experimental analysis protocol that relies on the above analysis. The accuracy of Eqs. (23), (24) and (27) will be numerically scrutinized in the following sections.

3. Finite element simulations

Two dimensional axisymmetric finite element simulations are performed to investigate the elastic indentation response of cones on materials with various Poisson's ratios, with emphasis being placed on auxeticity. The indenter was modeled as a rigid cone with half-apex angle of $\theta=70.3°$. This conical angle ensures the same contact depth vs. projected area of contact relation ($A_c=f(h_c)$) as in Vickers and Berkovich pyramidal indenters which are commonly employed in experimental investigations. Previous numerical studies by King (1987) showed that the assimilation of three-(Berkovich) and four-sided (Vickers) pyramidal indenters with a cone of equivalent semi-apex angle is accurate within 1–3%. Details of the model geometry are shown in Fig. 1. The 'semi-infinite' half-space is modeled as a 101 × 101 μm^2 linear elastic isotropic domain characterized by Young's modulus (E) and the Poisson ratio (ν). The indentation simulations were restricted to depths below 500 nm, much smaller than the domain such as to avoid any boundary effects. The continuum space is discretized using 4-node axisymmetric, isoparametric elements (CAX4–full integration). The element size was continuously refined in five successive regions (Fig. 1(b)) as approaching the indenter contact region for greater accuracy. A mesh sensitivity analysis was performed to ensure that the simulations results were insensitive to the mesh size. The computational contact was modeled using an analytic rigid surface for the probe and an element based surface for the contacting material, ensuring an accurate calculation of contact stresses at each node. The contact formulation includes the use of a constrained enforcement method for the pair surfaces of the master (indenter) – slave (sample) and accounts for finite strain, rotations and sliding. This direct method of Lagrange multipliers attempts to strictly enforce a given pressure-overclosure behavior per constraint.

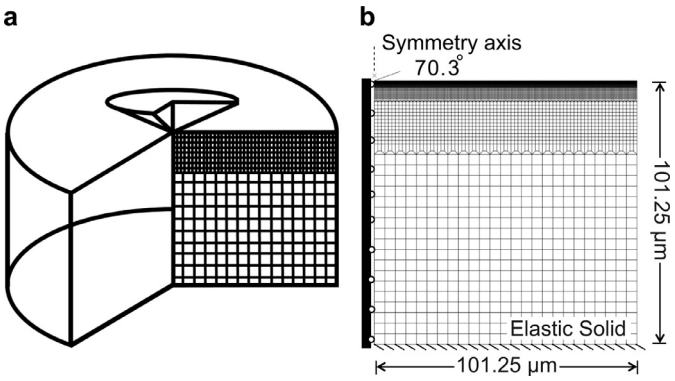

Fig. 1. (a) Schematic of the geometry modeled in this study. (b) Details of the mesh used.

Lagrange multipliers can add to the computational cost but also protect against numerical errors related to ill-conditioning that can occur if high contact stiffness is in effect. Any Lagrange multipliers associated with contact, are present only for active contact constraints so the number of equations will change as the contact status changes. By using this method, Lagrange multipliers are automatically selected based on the calculated stiffness (Abaqus, 2012). Frictional effects in the indenter–material interface were included in the analysis through an isotropic Coulomb model, in which the local shear stress τ_c is related to the local normal pressure p_c through $\tau_c = \mu p_c$ where μ is the friction coefficient between the indenter and the surface. We assume that the loading rate is slow enough such as static friction can securely model the interface response. Simulations proceeded in two steps: the indenter was firstly subjected to a ramped vertical displacement, followed by an indenter retraction to the original position which corresponded to complete unloading at zero load. During this process the lower edge of the material was constrained vertically. Axisymmetric boundary conditions were used along the symmetry axis beneath the indenter region (Sarris and Constantinides, 2013).

4. Results and discussion

4.1. Indentation resistance of auxetic materials

Fig. 2 shows the evolution of simulated $P-h$ responses for materials with an elastic modulus arbitrarily set to $E = 100$ GPa and various Poisson's ratios. The computational results suggest that the indentation resistance increases when $\nu \neq 0$. While a small increase is observed for positive Poisson's ratio (Fig. 2(a)) the resistance of the material significantly increases as the Poisson's ratio moves into the negative regime (Fig. 2(b)).

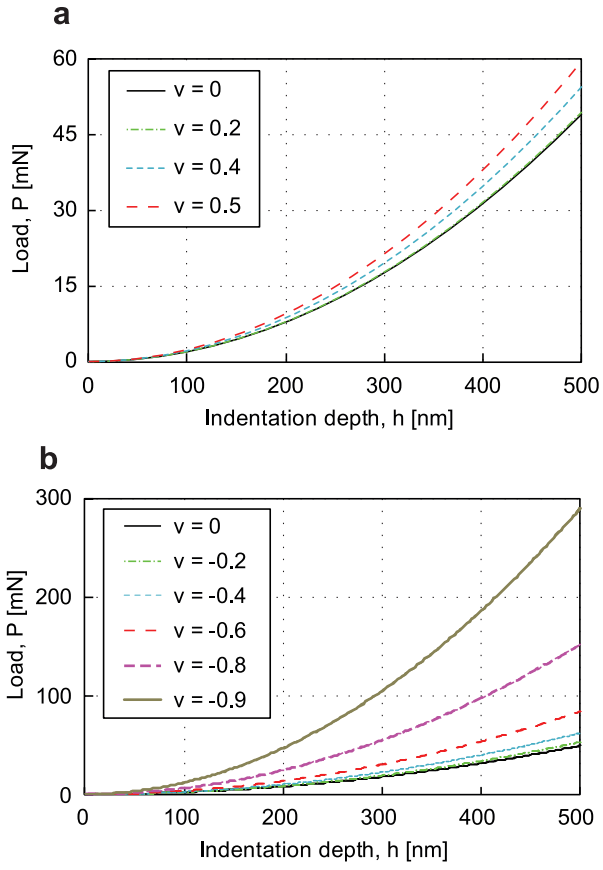

Fig. 2. Computational force-depth (P–h) responses for materials with $E = 100$ GPa and v in the (a) positive (0 to 0.5) and (b) negative (−1 to 0) regime.

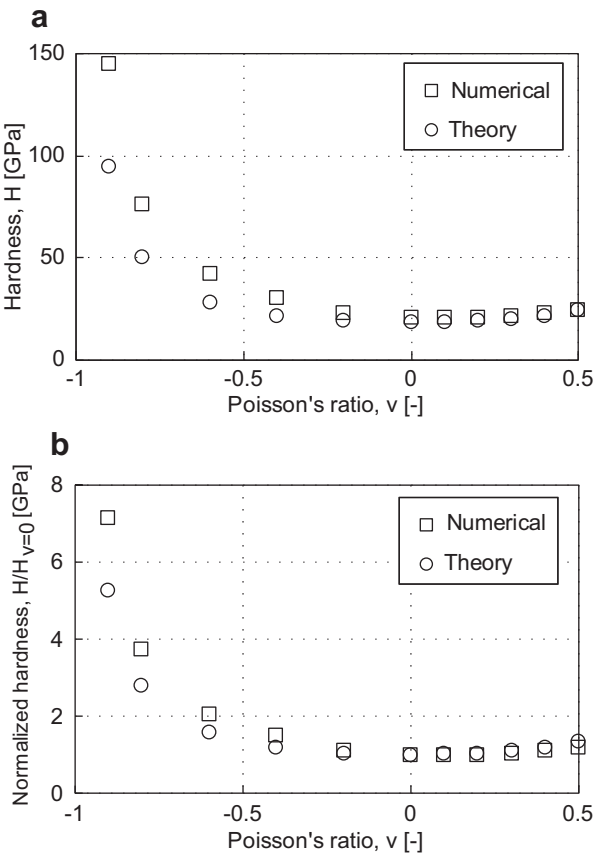

Fig. 3. Normalized hardness for various Poisson's ratios.

In order to better quantify the influence of ν on the material's ability to resist penetration we have calculated the elastic hardness of the material in the whole possible span of ν, $-1 \leq \nu \leq 0.5$ (Fig. 3). The physical meaning of hardness for elastic materials signifies their ability to resist penetration by a probe and relates to the average pressure generated beneath the indenter tip. Fig. 3(a) presents the numerical and theoretical hardness: the numerical results are calculated using Eq. (2) where P and A_c are numerically estimated, whereas the theoretical predictions conform to Eq. (24). It is observed that, with the exception of $\nu = 0.5$, the numerical results are consistently higher than the analytical solution. Furthermore, their deviation becomes more significant as ν reduces. The origins of this discrepancy will be further explored in the following sections.

Data in Fig. 3(b) corresponds to the normalized results of Fig. 3(a) by the hardness for $\nu = 0$ such as to present the relative

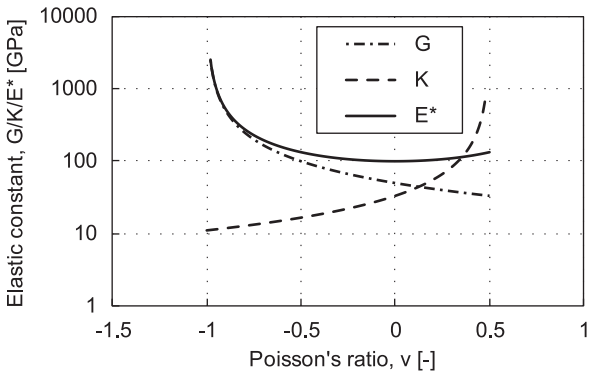

Fig. 4. Evolution of elastic material constants as a function of Poisson's ratio ($E = 100$ GPa).

amplification factor that the material experiences compared to the value at $\nu = 0$. Consistent with $P - h$ responses, the minimum possible resistance to penetration is provided for $\nu = 0$ and hardness increases for any deviation. The maximum within the positive regime is obtained for incompressible materials $\nu = 0.5$, $H/H_{\nu=0} = 1.17$ (numerical results). Of particular interest is the rapid amplification of hardness observed into the negative regime (auxetic materials) for which a sevenfold enhancement for the lowest ν simulated in this study ($H/H_{\nu=0} = 7.13$ for $\nu = -0.9$) is observed, distinctly different than the fivefold increase predicted by the analytical solution

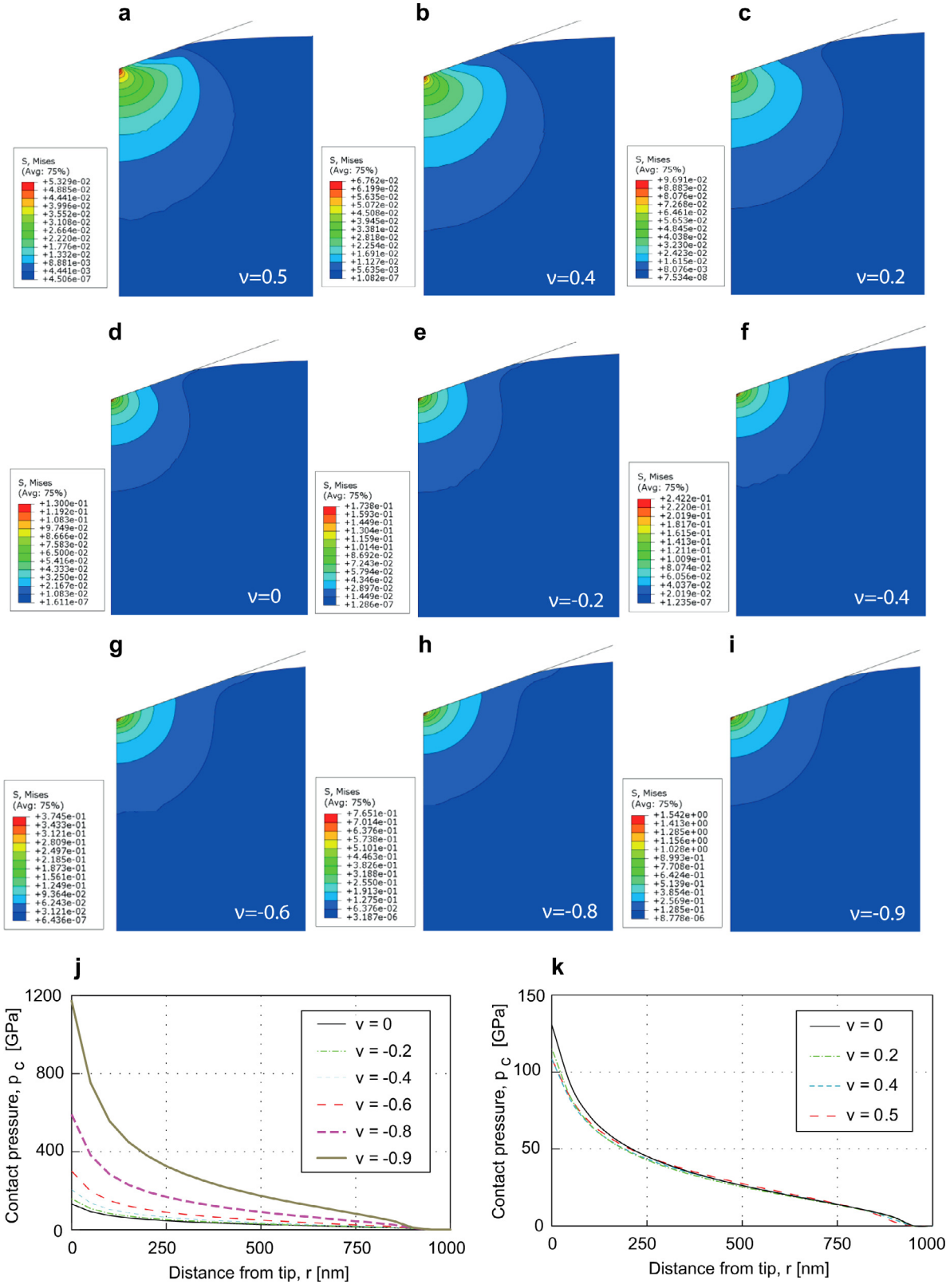

Fig. 5. (a)–(i) Von-Mises stress-profiles for the various Poisson's ratios ($\nu = 0.5, 0.4, 0.2, 0, -0.2, -0.4, -0.6, -0.8, -0.9$). Contact pressure distributions for negative (j) and positive (k) Poisson's ratios. The elastic modulus of the material is kept constant at $E = 100$ GPa.

($H/H_{\nu=0} = 5.26$ for $\nu = -0.9$). The ability of the material to enhance its resistance to penetration is consistent with the experimental observations reported in Alderson et al. (2000) and (1994). Before proceeding with a quantitative comparison between theory, simulations and experiments a few words on the nature of the indentation response of auxetic systems is due. In search of the physical mechanisms that lead to this amplified response we have investigated the interdependence of the elastic constants, the stress distributions beneath the indenter, and the contact depth evolution with Poisson's ratio.

Fig. 4 assists the interpretation of the previously reported results by plotting the evolution of the three elastic constants (K, G, $E*$) as a function of ν. The relations between K, G and ν are given by classical elasticity theory:

$$G = \frac{E}{2(1+\nu)};\ K = \frac{E}{3(1-2\nu)} \tag{28}$$

The analytical solution (Eq. (23)) suggests that the plane stress modulus, $E^* = E/(1-\nu^2)$, controls the indentation resistance of the material. It is evident that $E*$ experiences a minimum at $\nu = 0$ and increases for all other values. The increase is more significant in the negative Poisson's ratio domain especially for values of $\nu < -0.5$, below which $E*$ approaches the response of the shear modulus and together, thereafter, asymptotically increase to infinity as ν approaches –1. The transition to low ν values can therefore be interpreted as a shear-stiffening mechanism that also has implications on the indentation response. The limiting responses of the elastic constants are summarized below:

$$\nu \to 0.5:\ G \to \frac{E}{3},\ K \to \infty,\ E^* \to \frac{4}{3}E \tag{29}$$

$$\nu \to -1:\ G \approx E^* \to \infty,\ K \to \frac{E}{9} \tag{30}$$

Fig. 5 shows the von Mises stress – which relates to the distortional energy of the material – profiles for the various Poisson's ratio materials. It appears that as ν reduces, the resistance to penetration increases. This is manifested in (a) an increase in the absolute values of stresses generated within the indented material and (b) an increase in the normal stresses generated on the tip surface. These observations are consistent with the increase of maximum force required to penetrate lower Poisson's ratio materials to the same depth as observed in the simulated $P-h$ responses (see Fig. 2).

Fig. 6(a) presents the fully loaded deformed surface profiles and Fig. 6(b) indicates the numerically estimated contact depth normalized by the maximum indentation depth (here constant at $h =$ 500 nm) for the various Poisson's ratio materials. For positive Poisson's ratio materials, $h_c/h_{\max}$ appears to be relatively constant and in close agreement with theoretical prediction $h_c/h_{\max} = 2/\pi = 0.64$ (to two decimal places). The response assumes identical values to the theoretical prediction as the material approaches an incompressible system ($\nu = 0.5$). In that particular case the physical problem converges to the assumed boundary conditions of the analytical solution. It is interesting to observe that as Poisson's ratio moves into the negative regime (auxetic response) the normalized contact depth reduces, reaching a value of $h_c/h_{\max} = 0.57$ for $\nu = -0.9$. This response which cannot be captured analytically due to the ill-posed boundary condition can probably be attributed to the tendency of the material to 'shrink' (reduce its volume) under the high compressive stresses generated by the tip, with a subsequent reduction in the contact area. This reduction of contact depth, and subsequently contact area, is in part responsible for the increased hardness observed in the negative Poisson's ratio regime.

Based on the above analysis and recalling Eq. (2) one can therefore trace the enhanced indentation resistance offered by auxetic systems to (a) the shear stiffening response which leads to increased required load for penetration and (b) the reduced area of contact that

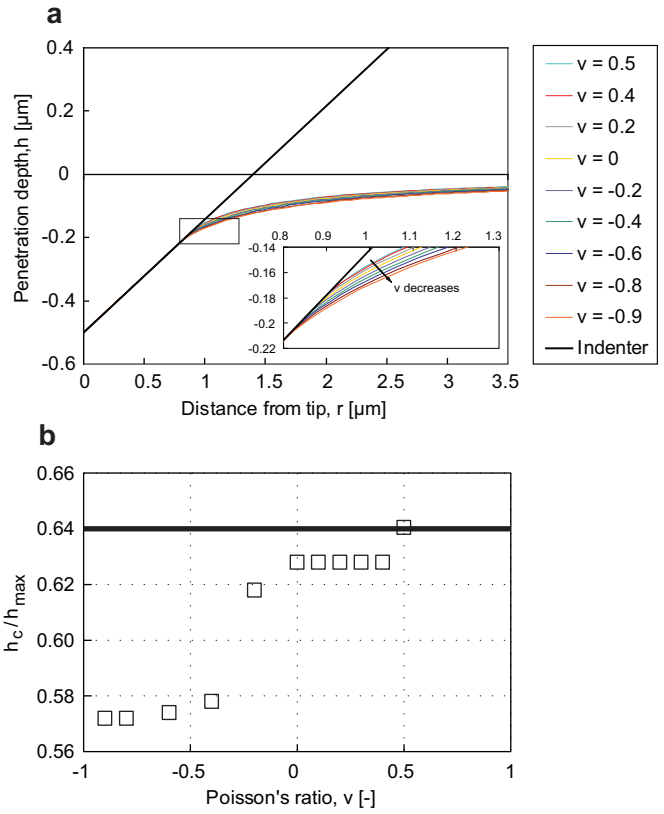

Fig. 6. (a) Surface profiles at maximum depth of penetration for various Poisson's ratios. (b) Normalized contact depth for various Poisson's ratios.

leads to higher stresses beneath the indenter tip. A literature search on available experimental indentation data on auxetic materials revealed a limited number of publications on the subject, all of which have used cylindrical or spherical indenters to probe the material. Strictly speaking, hardness is not a material property but rather a snapshot of material properties; it subsequently depends on many factors among them the geometry of the tip. One should, therefore, not expect that the hardness of the material obtained with a spherical tip would correspond to the hardness of the material obtained with a conical tip. Nevertheless, theoretical solutions for both geometries exist that provide estimates of the amplification of elastic hardness as a function of the Poisson's ratio: $\frac{H}{H_{\nu=0}} = (1-\nu^2)^{-1}$ for cones and $\frac{H}{H_{\nu=0}} = (1-\nu^2)^{-2/3}$ for spheres. The theoretical discrepancy between the hardness amplifications obtained by the two

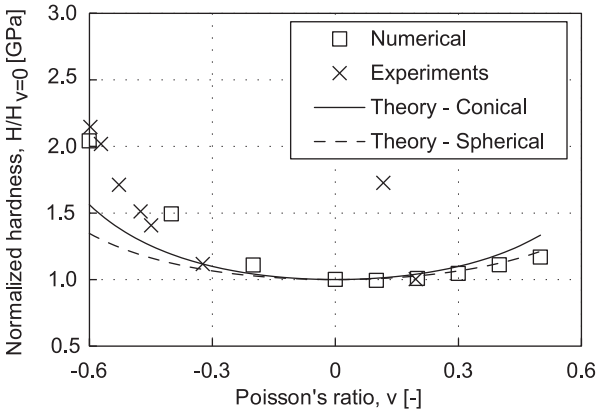

Fig. 7. Theoretical, numerical and experimental (data from Alderson et al. (1994)) results of normalized hardness for various Poisson's ratio materials. The experimental outlier (for $\nu \approx 0.1$) corresponds to a sintered material.

geometries is expected to increase as ν moves away from $\nu = 0$: within $-0.5 < \nu < 0.5$ the maximum error is contained within ±9% (due to symmetry around $\nu = 0$), for $\nu = -0.6$ it grows to 14% and for $\nu = -0.8$ to 30%. Given the relatively small discrepancies (maximum of 14%) predicted within $-0.6 < \nu < 0.5$ we decided to present the experimental data from spherical indentation and contrast them to the numerical results computed in this study, having in mind in parallel the limitations presented above. Alderson et al. (1994) performed spherical indentation data on auxetic polyethylene. The auxetic materials consisted of microporous ultra high molecular weight polyethylene (UHMWPE) that have been fabricated through a three-stage thermal route (Alderson et al., 1994). Materials with Poisson's ratios down to –0.8 have been synthesized and tested under spherical (5 mm diameter ball) indentation. Results with axial loads of 25, 50, 100 and 200N have been presented. It was reported that high values of axial loads led to non-linear phenomena caused by large strains, plasticity and anisotropy. We here include the data collected with 25N axial load which ensures the elastic response of the system. Experimental data, theoretical predictions and numerical simulations are plotted in Fig. 7. It is interesting to note that the experimental data shows a hardness enhancement higher than the theoretical predictions of both conical and spherical indentation, approaching the numerically simulated response. While this observation is encouraging regarding the validity of our results, additional experiments

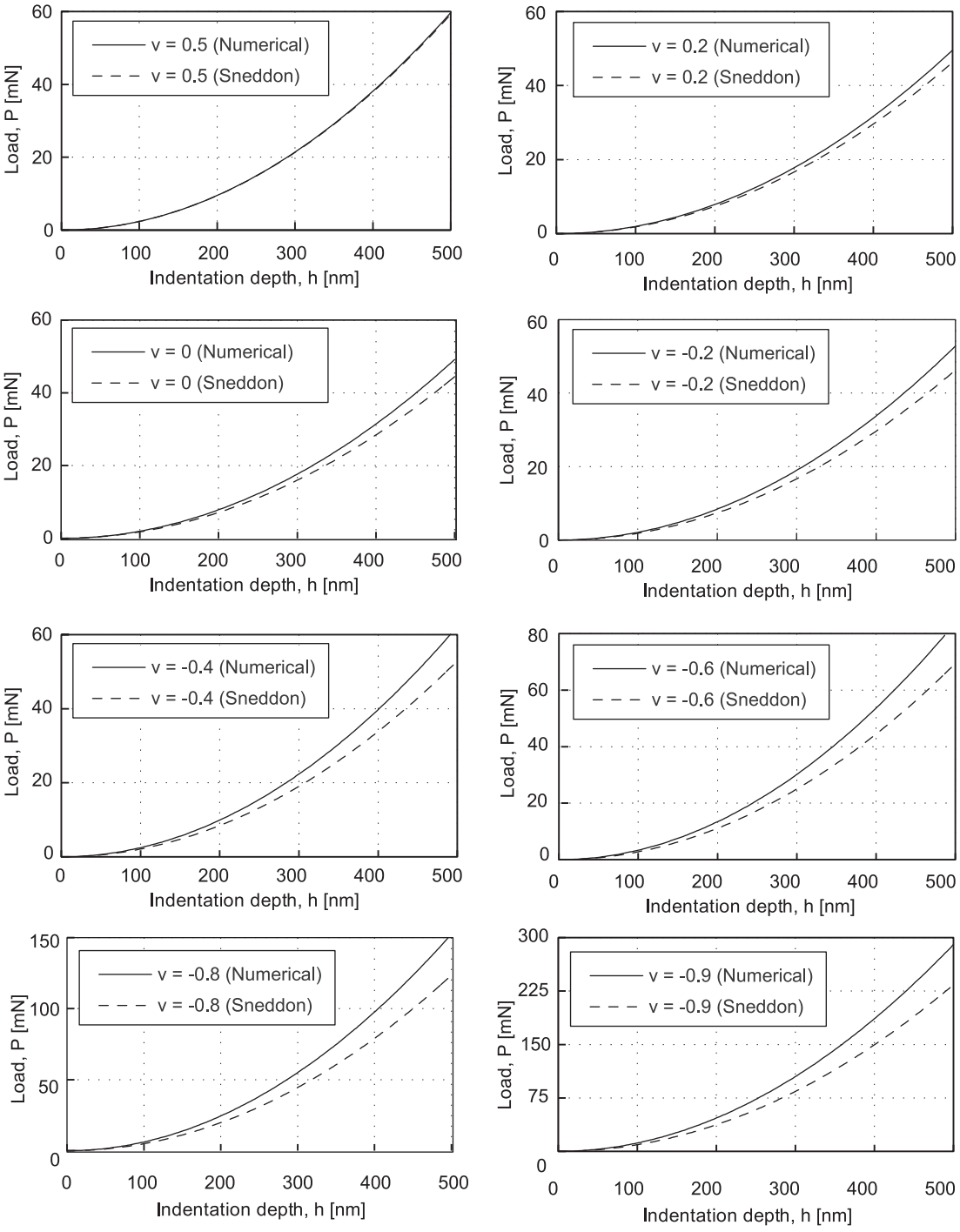

Fig. 8. Analytical and computational force–depth (P–h) responses for materials with $E = 100$ GPa and ν in the range of 0.5 to –1.

are required in order to confirm this scaling relation. While not presented here, it is interesting to note that the experimental data even for lower Poisson's ratios ($\nu < -0.6$) is in close agreement with our simulations. Nevertheless, the interpretation of this data should be treated with caution given the discrepancy that might be included from the spherical geometry used in those experiments.

4.2. Correction factor for the analytical solution

The simulated $P-h$ responses presented in Fig. 2 can also be predicted by the analytical solution of Sneddon, Eq. (23). Fig. 8 contrasts the analytical and numerical results for the various Poisson's ratios. The discrepancy between the two increases as Poisson's ratio decreases. This phenomenon has firstly been reported by Hay et al. (1999) in the positive Poisson's ratio regime and has been attributed to the ill-posed boundary conditions of the analytical problem formulation which results in a deformed material surface shape that penetrates into the indenter. In this section we compute the correction factor for the whole possible span of Poisson's ratios and we also investigate the effect of friction and indenter angles.

It is interesting to note that the error observed in the load is constant throughout the depth of indentation suggesting that a multiplicative correction factor on Sneddon's equation will resolve the observed discrepancy:

$$P = \gamma \frac{\pi}{2} \frac{E}{1-\nu^2} \tan\theta h^2 \tag{31}$$

This load discrepancy propagates into the fundamental equations used for calculating the elastic modulus and hardness of the material during a nanoindentation experiment. Eqs. (1) and (2) can therefore also be corrected using γ:

$$E^* = \frac{1}{\gamma} \frac{\sqrt{\pi}}{2} \frac{S}{\sqrt{A_c}} \tag{32}$$

$$H = \gamma \frac{P_{\max}}{A_c} \tag{33}$$

From a materials perspective it appears that the correction factor is independent of the elastic modulus of the material. We have checked the correction factor for three different elastic moduli, $E = 1$ GPa, 10 GPa, 100 GPa with nearly identical results. The most notable influence comes from Poisson's ratio of the material (Fig. 9). As ν reduces the discrepancy between the numerical results and the analytical solution increase, with higher deviations observed in the negative Poisson's ratio regime with values reaching up to 23% for the lowest possible ν that has been simulated in this study ($\nu = -0.9$). For positive ν the error is contained below 10% with the results between theory and simulations to converge when $\nu \to 0.5$ (incompressible media). The numerical results of Hay et al. (1999) and Poon et al. (2008) and the analytical formulation proposed by Hay et al. (Eq. (4)) are also presented in Fig. 9 and compare favorably with our simulations, with the observed deviations being within 1% and could be potentially attributed to numerical details between the different studies.

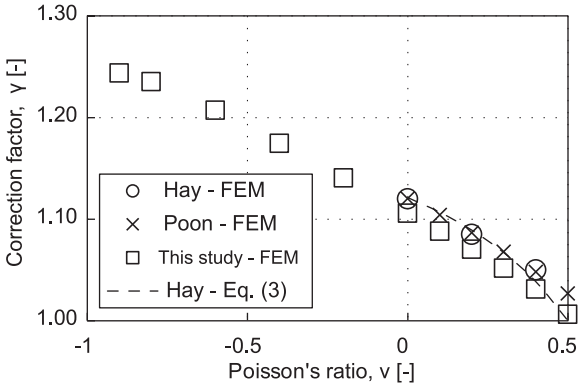

Fig. 9. Correction factor for various Poisson's ratios.

4.3. Effect of friction

The contact friction between the indenter and indented materials has been simulated at three different values: $\mu = 0, 0.5, 1$. Fig. 10(a) suggests that the $P-h$ response remains mostly unaffected to the contact friction. A similar response is observed on the correction factor scaling function in which the presence of friction shifts the curve slightly upwards with the maximum observed deviation being in the order of 5% for the lowest simulated ν. The mathematical problem of adhesive contact by a flat punch has been analytically treated by Mossakovskii in 1954 (see references in (Borodich and Keer, 2004a, 2004b)) who has later extended his solution to parabolic and spherical punches (Mossakovskii, 1963). The geometry of cone, that pertains to our case, has been tackled by Spence (1968). More recently, building on the early mathematical developments of Mossakovksii, the results of adhesive (non-slip) indentation have been generalized by Borodich and Keer to any probe that can be described by a monomial shape (Borodich and Keer, 2004a, 2004b). They concluded that the results on adhesive conical indentation on a semi-infinite half space are similar to the frictionless case but with a correction factor γ^{ad} that is introduced in the relation between the contact stiffness and the elastic modulus of the material:

$$S = \frac{dP}{dh} = \gamma^{ad} \frac{2E}{1-\nu^2} \frac{\sqrt{A_c}}{\sqrt{\pi}} \tag{34}$$

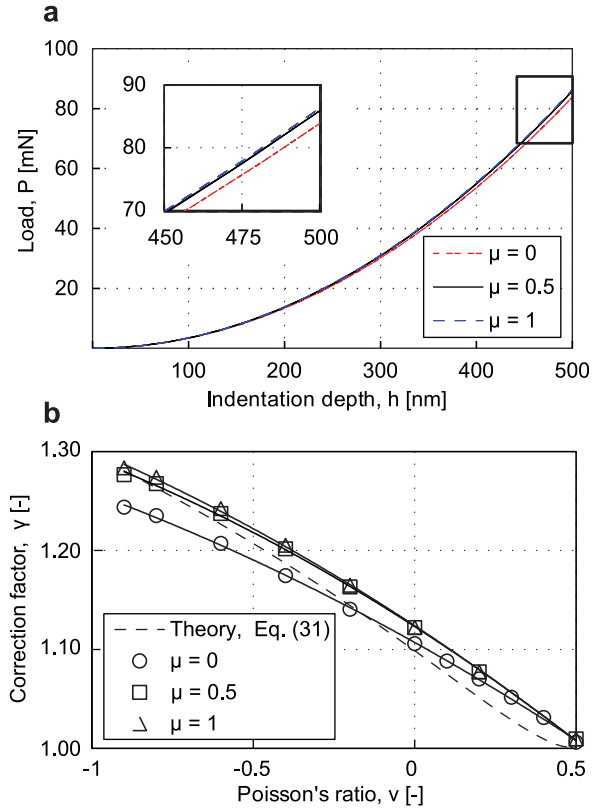

Fig. 10. (a) P–h curves for three different coefficients of friction: $\mu = 0, 0.5, 1$. Inset represents a magnified region on the highest load/depth area. (b) The dependency of the correction factor on Poisson's ratio is computed for three different coefficients of friction: $\mu = 0, 0.5, 1$. Solid lines represent polynomial fits.

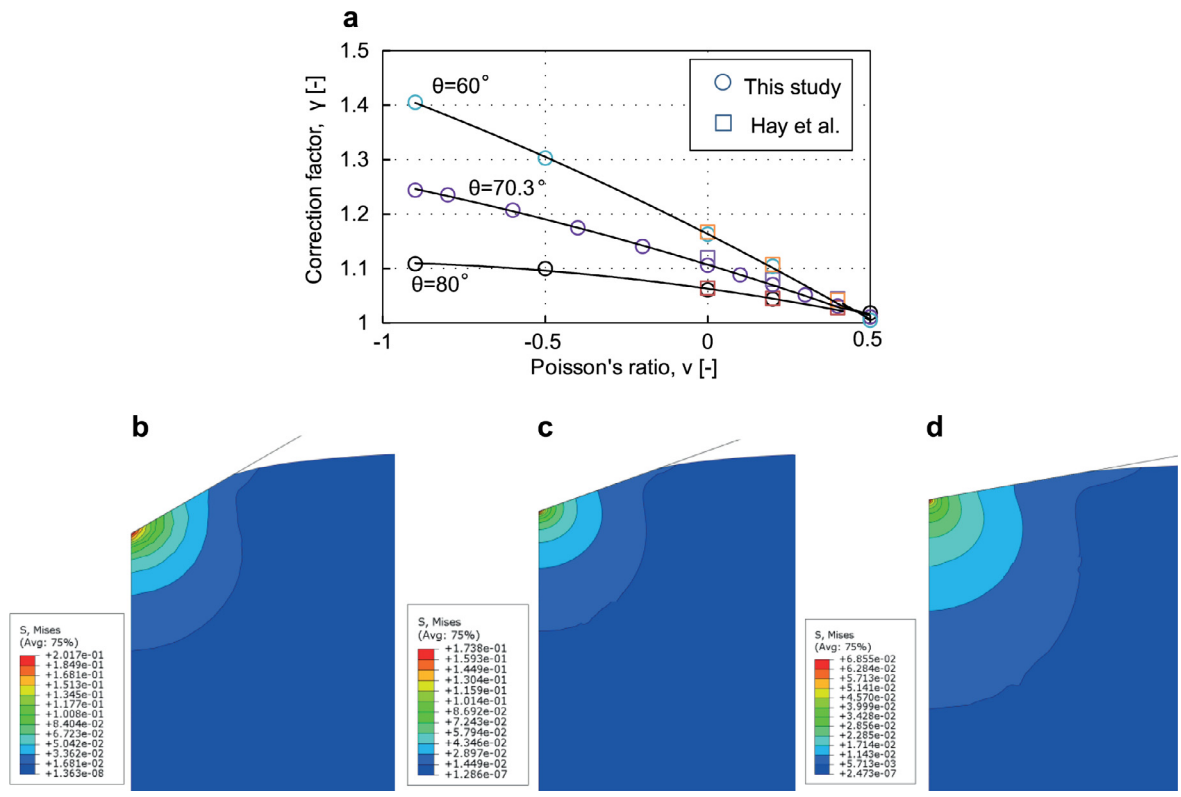

Fig. 11. (a) The dependency of the correction factor on Poisson's ratio is computed for three different cone half-apex angles: $\boldsymbol{\theta} = 60°, 70.3°, 80°$. Solid lines represent polynomial fits. Von Mises stress fields for three different cone half-apex angles: (b) $\boldsymbol{\theta} = 60°$, (c) 70.3°, (d) 80°.

where γ^{ad} is the correction factor for the case of adhesive (no-slip) contact of a rigid probe (Borodich and Keer, 2004a, 2004b):

$$\gamma^{ad} = \frac{\ln(3-4\nu)}{\beta} \tag{35}$$

Eq. (35), which is included in Fig. 10(b) compares well with the simulated results suggesting that the actual deformed geometry in the presence of friction is much closer to the assumed boundary condition of the analytical solution (minimal radial displacements) resulting in significantly reduced discrepancies compared to the frictionless case

4.4. Effect of indenter angle

Results on the correction factor for three different indenter geometries ($\theta = 60°, 70.3°, 80°$) are plotted in Fig. 11(a). The results of Hay et al., 1999 for positive ν are also included for comparison. The data collected in this study is in excellent agreement with previously published results confirming the accuracy of the simulations. Furthermore, the data extends the correction factor into the negative regime in which the discrepancy becomes more severe. Overall, it appears that γ decreases with decreasing cone angle and/or increasing ν. All of the geometries converge to the theoretical solution for $\nu = 0.5$. The correction factor also vanishes as the cone angle approaches 90° consistent with the boundary condition of the analytical solution in which radial displacements are eliminated. The stress profiles for $\nu = -0.2$ and three different indenter geometries are shown in Fig. 11(b)–(d). Since the load scales with the area of contact, blunt indenters, in which the area-to-depth scaling relation is more rapid, tend to offer more resistance to penetration. This however is accompanied with a load-spreading over a larger area and a subsequent smoothing/reduction of the stress distribution/intensity over the indenter-material contact region.

5. Concluding remarks

Consistent with theoretical predictions, auxetic materials enhance their indentation resistance especially for Poisson's ratio's approaching $\nu \to -1$. This amplified response can be attributed to a shear stiffening phenomenon and an associated material miotic response (shrinking) beneath the indenter region with a subsequent reduction in the contact area. The hardness enhancement as predicted by the numerical simulations presented in Fig. 3(b) for a 70.3° conical indenter (Berkovich equivalent), can be approximated by:

$$H/H_{\nu=0} = \left(1-\nu^2\right)^{-1.193};\ R^2 = 0.9887 \tag{36}$$

Eq. (36) has the same form as predicted by the analytical solution ($\frac{H}{H_{\nu=0}} = (1-\nu^2)^k$) but with a different best-fitted k exponent to

Table 1
Best fit polynomials for Poisson's ratio dependency of the correction factor γ.

Cone semi-apex angle, θ [°]	Friction coefficient, μ [dimensionless]	Polynomial fit
70.3	0	$\gamma = 1.1070 - 0.1821\nu - 0.0306\nu^2$; $R^2 = 0.9996$
70.3	0.5	$\gamma = 1.1231 - 0.2106\nu - 0.0406\nu^2$; $R^2 = 0.9995$
70.3	1	$\gamma = 1.1240 - 0.2145\nu - 0.0369\nu^2$; $R^2 = 0.9994$
80	0	$\gamma = 1.0629 - 0.0842\nu - 0.0357\nu^2$; $R^2 = 0.9960$
60	0	$\gamma = 1.1633 - 0.3033\nu - 0.0396\nu^2$; $R^2 = 0.9998$

capture the corrected indentation hardness enhancement as calculated through numerical simulations. The assumptions incorporated in the analytical solutions of a rigid axisymmetric probe being pushed against a semi-infinite linear elastic half-space become increasingly inaccurate for elastic indentations on auxetic materials ($\nu < 0$). The linear elastic solution for load (Eq. (31)), contact stiffness (Eq. (32)) and elastic hardness (Eq. (33)) that form the basis for many experimental data analysis protocols can be corrected to account for the effect of Poisson's ratio, contact angle and contact friction. The polynomial correction functions $\gamma = f(\nu)$ (valid for $-1 \leq \nu \leq 0.5$) calculated in this study and which can serve in eliminating errors during experimental investigations are summarized in Table 1.

Acknowledgments

The authors would like to acknowledge the financial support from the Strategic Infrastructure Project NEW INFRASTRUCTURE/STRATE/0308/04 of DESMI 2008, which is co-financed by the European Regional Development Fund, the European Social Fund, the Cohesion Fund, and the Research Promotion Foundation of the Republic of Cyprus. GC and ES would also like to acknowledge the financial support from Cyprus University of Technology start-up grant.

References

Abaqus, 2012. Abaqus Analysis User's Manual. Dassault Systèmes, Providence, RI, USA.
Alderson, K.L., Fitzgerald, A., Evans, K.E., 2000. The strain dependent indentation resilience of auxetic microporous polyethylene. J. Mater. Sci. 5, 4039–4047.
Alderson, K.L., Pickles, A.P., Neale, P.J., Evans, K.E., 1994. Auxetic polyethylene: the effect of a negative Poisson's ratio on hardness. Acta Metall. Mater. 42, 2261–2266.
Argatov, I.I., 2004. Approximate solution of an axisymmetric contact problem with allowance for tangential displacements on the contact surface. J. Appl. Mech. Tech. Phys. 45, 118–123.
Argatov, I.I., Guinovart-Díaz, R., Sabina, F.J., 2012. On local indentation and impact compliance of isotropic auxetic materials from the continuum mechanics viewpoint. Int. J. Eng. Sci. 54, 42–57.
Argatov, I.I., Sabina, F.J., 2014. Small-scale indentation of an elastic coated half-space: influence of Poisson's ratios on the substrate effect. Int. J. Eng. Sci. 81, 33–40.
Bolshakov, A., Pharr, G.M., 1998. Influences of pileup on the measurement of mechanical properties by load and depth sensing indentation techniques. J. Mater. Res. 13, 1049–1058.
Borodich, F.M., 2014. The Hertz-type and adhesive contact problems for depth-sensing indentation. Adv. Appl. Mech. 47, 225–366.
Borodich, F.M., Keer, L.M., 2004a. Contact problems and depth-sensing nanoindentation for frictionless and frictional boundary conditions. Int. J. Solids Struct. 41, 2479–2499.
Borodich, F.M., Keer, L.M., 2004b. Evaluation of elastic modulus of materials by adhesive (no-slip) nano-indentation. Proc. R. Soc. A Math. Phys. Eng. Sci. 460, 507–514.
Bulychev, S.I., Alekhin, V.P., Shorshorov, M.K., Ternovskii, A.P., Shnyrev, G.D., 1975. Determination of Young's modulus according to the indentation diagram. Ind. Lab. 41, 1409–1412.
Cariou, S., Ulm, F.-J., Dormieux, L., 2008. Hardness–packing density scaling relations for cohesive-frictional porous materials. J. Mech. Phys. Solids 56, 924–952.
Cheng, C.-M., Cheng, Y.-T., 1997. On the initial unloading slope in indentation of elastic-plastic solids by an indenter with an axisymmetric smooth profile. Appl. Phys. Lett. 71, 2623.
Cheng, Y.-T., Cheng, C.-M., 1999. Scaling relationships in conical indentation of elastic-perfectly plastic solids. Int. J. Solids Struct. 36, 1231–1243.
Cheng, Y.-T., Cheng, C.-M., 1998. Analysis of indentation loading curves obtained using conical indenters. Philos. Mag. Lett. 77, 39–47.
Constantinides, G., Chandran, Ravi K.S., Ulm, F.-J., Van Vliet, K.J., 2006. Grid indentation analysis of composite microstructure and mechanics: principles and validation. Mater. Sci. Eng. A 430, 189–202.
Constantinides, G., Smith, J.F., Ulm, F.-J., 2009. Nanomechanical explorations of cementitious materials: recent results and future perspectives. In: Bittnar, Z., Bartos, P.J.M., Němeček, J., Šmilauer, V., Zeman, J. (Eds.), Nanotechnology in Construction 3. Springer, pp. 63–69.
Constantinides, G., Ulm, F.-J., Van Vliet, K.J., 2003. On the use of nanoindentation for cementitious materials. Mater. Struct. 36, 191–196.
Cook, R.F., Pharr, G.M., 1990. Direct observation and analysis of indentation cracking in glasses and ceramics. J. Am. Ceram. Soc. 73, 787–817.
Dao, M., Chollacoop, N., Van Vliet, K.J., Venkatesh, T.A., Suresh, S., 2001. Computational modeling of the forward and reverse problems in instrumented sharp indentation. Acta Mater 49, 3899–3918.
Doerner, M.F., Nix, W.D., 1986. A method for interpreting the data from depth-sensing indentation instruments. J. Mater. Res. 1, 601–609.
Fischer-Cripps, A.C., 2002. Nanoindentation, Mechanical Engineering Series. Springer, New York, New York, NY.
Ganneau, F.P., Constantinides, G., Ulm, F.-J., 2006. Dual-indentation technique for the assessment of strength properties of cohesive-frictional materials. Int. J. Solids Struct. 43, 1727–1745.
Gatt, R., Zammit, V., Caruana, C., Grima, J.N., 2008. On the atomic level deformations in the auxetic zeolite natrolite. Phys. Status Solidi. 245, 502–510.
Greaves, G.N., Greer, A.L., Lakes, R.S., Rouxel, T., 2011. Poisson's ratio and modern materials. Nat. Mater. 10 986–986.
Grima, J.N., Gatt, R., Alderson, A., Evans, K.E., 2005. On the origin of auxetic behaviour in the silicate α-cristobalite. J. Mater. Chem. 15, 4003.
Grima, J.N., Winczewski, S., Mizzi, L., Grech, M.C., Cauchi, R., Gatt, R., Attard, D., Wojciechowski, K.W., Rybicki, J., 2015. Tailoring graphene to achieve negative Poisson's ratio properties. Adv. Mater. 27, 1455–1459.
Hay, J.C., Bolshakov, A., Pharr, G.M., 1999. A critical examination of the fundamental relations used in the analysis of nanoindentation data. J. Mater. Res. 14, 2296–2305.
Kindrachuk, V.M., Galanov, B.A., Kartuzov, V.V., Dub, S.N., 2009. Refined model of elastic nanoindentation of a half-space by the blunted Berkovich indenter accounting for tangential displacements on the contact surface. J. Mater. Sci. 44, 2599–2609.
King, R.B., 1987. Elastic analysis of some punch problems for a layered medium. Int. J. Solids Struct. 23, 1657–1664.
Lakes, R., 1993. Advances in negative Poisson's ratio materials. Adv. Mater. 5, 293–296.
Lakes, R., 1987. Foam structures with a negative Poisson's ratio. Science 235, 1038–1040.
Lawn, B.R., 1998. Indentation of ceramics with spheres: a century after Hertz. J. Am. Ceram. Soc. 94, 1977–1994.
Lee, E.H., Radok, J.R.M., 1960. The contact problem for viscoelastic bodies. J. Appl. Mech. 27, 438.
Milton, G.W., 1992. Composite materials with Poisson's ratios close to –1. J. Mech. Phys. Solids 40, 1105–1137.
Mossakovskii, V.I., 1963. Compression of elastic bodies under conditions of adhesion (axisymmetric case). J. Appl. Math 27, 630–643.
Němeček, J., Králík, V., Vondřejc, J., 2013. Micromechanical analysis of heterogeneous structural materials. Cem. Concr. Compos. 36, 85–92.
Oliver, W.C., Pharr, G.M., 2011. Measurement of hardness and elastic modulus by instrumented indentation: advances in understanding and refinements to methodology. J. Mater. Res. 19, 3–20.
Oliver, W.C., Pharr, G.M., 1992. An improved technique for determining hardness and elastic modulus using load and displacement sensing indentation experiments. J. Mater. Res. 7, 1564–1583.
Pharr, G.M., Oliver, W.C., Brotzen, F.R., 1992. On the generality of the relationship among contact stiffness, contact area, and elastic modulus during indentation. J. Mater. Res. 7, 613–617.
Poon, B., Rittel, D., Ravichandran, G., 2008. An analysis of nanoindentation in linearly elastic solids. Int. J. Solids Struct. 45, 6018–6033.
Sarris, E., Constantinides, G., 2013. Finite element modeling of nanoindentation on C-S-H: Effect of pile-up and contact friction. Cement Concrete Comp. 78–84.
Schuh, C.A., 2006. Nanoindentation studies of materials. Mater. Today 9, 32–40.
Sneddon, I.N., 2010. Fourier Transforms. Dover Publications.
Sneddon, I.N., 1965. The relation between load and penetration in the axisymmetric Boussinesq problem for a punch of arbitrary profile. Int. J. Eng. Sci. 3, 47–57.
Spence, D.A., 1968. Self-similar solutions to adhesive contact problems with incremental loading. Proc. R. Soc. A Math. Phys. Eng. Sci. 305, 55–80.
Tabor, D., 2000. The hardness of metals. Oxford Classic Texts. Oxford Classic Texts.
Troyon, M., Huang, L., 2011. Correction factor for contact area in nanoindentation measurements. J. Mater. Res. 20, 610–617.
Tweedie, C.A., Constantinides, G., Lehman, K.E., Brill, D.J., Blackman, G.S., Van Vliet, K.J., 2007. Enhanced stiffness of amorphous polymer surfaces under confinement of localized contact loads. Adv. Mater. 19, 2540–2546.
Vandamme, M., Tweedie, C.A., Constantinides, G., Ulm, F.-J., Van Vliet, K.J., 2012. Quantifying plasticity-independent creep compliance and relaxation of viscoelastoplastic materials under contact loading. J. Mater. Res. 27, 302–312.
VanLandingham, M.R., Villarrubia, J.S., Guthrie, W.F., Meyers, G.F., 2001. Nanoindentation of polymers: an overview. Macromol. Symp. 167, 15–44.
Wachtman, J.B., Cannon, W.R., Matthewson, M.J., 2009. Mechanical Properties of Ceramics. John Wiley & Sons.
Xu, Z., 2008. Effects of indenter geometry and material properties on the correction factor of Sneddon's relationship for nanoindentation of elastic and elastic–plastic materials. Acta Mater 56, 1399–1405.
Yang, W.E.I., Li, Z., Shi, W.E.I., Xie, B., Yang, M., 2004. On auxetic materials. Review on Auxetic Materials 9, 3269–3279.
Zouboulis, I.S., Jiang, F., Wang, J., Duffy, T.S., 2014. Single-crystal elastic constants of magnesium difluoride (MgF2) to 7.4 GPa. J. Phys. Chem. Solids 75, 136–141.